Journal of Computational Physics 262 (2014) 344–357

Contents lists available at ScienceDirect

Journal of Computational Physics

www.elsevier.com/locate/jcp

A characteristic based volume penalization method for general evolution problems applied to compressible viscous flows ☆

Eric Brown-Dymkoski, Nurlybek Kasimov, Oleg V. Vasilyev *

Department of Mechanical Engineering, University of Colorado Boulder, Boulder, CO 80309, USA

ARTICLE INFO

Article history:
Received 17 May 2013
Received in revised form 18 October 2013
Accepted 31 December 2013
Available online 15 January 2014

Keywords:
CFD
Immersed boundary method
Volume penalization
Compressible flow
Neumann boundary condition
Robin boundary condition

ABSTRACT

In order to introduce solid obstacles into flows, several different methods are used, including volume penalization methods which prescribe appropriate boundary conditions by applying local forcing to the constitutive equations. One well known method is Brinkman penalization, which models solid obstacles as porous media. While it has been adapted for compressible, incompressible, viscous and inviscid flows, it is limited in the types of boundary conditions that it imposes, as are most volume penalization methods. Typically, approaches are limited to Dirichlet boundary conditions. In this paper, Brinkman penalization is extended for generalized Neumann and Robin boundary conditions by introducing hyperbolic penalization terms with characteristics pointing inward on solid obstacles. This Characteristic-Based Volume Penalization (CBVP) method is a comprehensive approach to conditions on immersed boundaries, providing for homogeneous and inhomogeneous Dirichlet, Neumann, and Robin boundary conditions on hyperbolic and parabolic equations. This CBVP method can be used to impose boundary conditions for both integrated and non-integrated variables in a systematic manner that parallels the prescription of exact boundary conditions. Furthermore, the method does not depend upon a physical model, as with porous media approach for Brinkman penalization, and is therefore flexible for various physical regimes and general evolutionary equations. Here, the method is applied to scalar diffusion and to direct numerical simulation of compressible, viscous flows. With the Navier–Stokes equations, both homogeneous and inhomogeneous Neumann boundary conditions are demonstrated through external flow around an adiabatic and heated cylinder. Theoretical and numerical examination shows that the error from penalized Neumann and Robin boundary conditions can be rigorously controlled through an *a priori* penalization parameter η. The error on a transient boundary is found to converge as $O(\eta)$, which is more favorable than the error convergence of the already established Dirichlet boundary condition.

1. Introduction

Numerical simulations of complex geometry flows in a computationally efficient manner, especially for moving surfaces, is a challenging problem. Solid bodies are introduced by imposing appropriate boundary conditions upon surfaces, and to that end, several approaches are used. These methods can be separated into two major groups: body-fitted mesh and immersed boundary methods. The former uses grids with nodes coincident to the surface of an obstacle, while the latter employs forcing upon the constitutive equations to impose appropriate boundary conditions.

* Corresponding author.
E-mail address: Oleg.Vasilyev@Colorado.edu (O.V. Vasilyev).

0021-9991/$ – see front matter
http://dx.doi.org/10.1016/j.jcp.2013.12.060

Though body-conformal meshes allow for exact boundary conditions (BCs) to be imposed, the grid must be carefully constructed to precisely fit an obstacle. In most cases, this precludes the use of structured Cartesian grids. The process of mesh generation is highly dependent upon the obstacle geometry, and can become computationally expensive, especially for complex surfaces. This issue is compounded for moving or deforming obstacles, which require continuous adaptation or re-meshing throughout computation of the solution [1].

Immersed boundary methods avoid the cost and complications of body meshing by introducing the effects of obstacles upon the governing equations themselves. Solid body effects, thus embedded within the flow itself, obviate the rigors of positioning nodes upon a surface. Immersed boundary forcing can be applied either to the continuous or discretized equations. While applying discretized forcing allows for a high level of control based upon the numerical accuracy and conservative properties of the discretization method, this approach lacks generality and flexibility across solvers [1].

Volume penalization, on the other hand, imposes the effects of solid bodies by introducing forcing terms on the continuous equations and the resulting evolutionary equations are discretized and solved in the normal manner. One such method is the Brinkman Penalization Method (BPM) [2], which was originally developed for solid, isothermal obstacles in incompressible flows. A principal strength of Brinkman penalization is that error can be rigorously controlled *a priori*, with the solution converging to the exact in a predictable fashion [3,4]. Much work has been done to refine BPM for various numerical techniques, including pseudospectral methods [4–6], wavelets [7,8], and finite-element/finite-volume methods [9]. Of particular note is the impact of volume penalization upon pseudospectral methods, as it has allowed for arbitrary domain geometry and the ability to circumvent the limitations of periodic boundaries [5,6]. In addition to being extended to various solvers, BPM has been expanded beyond the original application of incompressible flows to compressible [7,10] and inviscid [11] regimes.

For all of this progress, boundary conditions imposed by BPM have lacked generality, especially for compressible flows. They have been typically limited to isothermal obstacles and slip/no-slip conditions for the inviscid and viscous regimes, respectively. Additional boundary conditions have been developed on an individual, and usually problem specific, basis. Though homogeneous Neumann condition was recently formulated for scalar mixing and advection–diffusion problems [12], general treatment of homogeneous/inhomogeneous Robin and Neumann conditions has been limited to finite-volume/finite-element methods [9]. In this way, BPM has been inapplicable for many fluid problems, notably those demanding heat-flux and insulating boundary conditions on solid surfaces.

In this work, we propose an extension of volume penalization that introduces characteristic-based forcing terms, exploiting their hyperbolicity to impose general homogeneous and inhomogeneous Neumann and Robin boundary conditions. This Characteristic-Based Volume Penalization (CBVP) method is flexible and can be applied to parabolic and hyperbolic evolutionary equations; in this paper, CBVP is examined for both scalar diffusion and the fully compressible Navier–Stokes equations. As with BPM, this method maintains rigorous control of the error through *a priori* chosen parameters for all boundary conditions.

Characteristic-based volume penalization is well suited for use with adaptive mesh refinement (AMR). As volume penalization does not require body-conformal meshing, high resolution is required around surfaces for computational accuracy and proper definition of geometry. The use of AMR grids maintains solid geometry resolution without over-resolving flow structures. Additionally, the number of nonphysical points lying inside of the obstacle can be minimized to those necessary to support the boundary conditions, which is particularly important for obstacles inhabiting a large portion of the computational domain. All of the results reported in this paper were obtained using the Adaptive Wavelet Collocation Method (AWCM), a general numerical solver which utilizes a wavelet decomposition to dynamically adapt on steep gradients in the solution while retaining a predetermined order of accuracy [13–15]. Employing a rectilinear grid, AWCM precludes the use of body-fitted meshes to impose solid obstacles for all but the most simple geometries. Therefore, volume penalization is a natural means for introducing solid obstacles. As the geometry definitions are treated as any other flow variable by AWCM, and the local grid efficiently and dynamically adapts to resolve surfaces, even for moving obstacles.

2. Characteristic-based volume penalization

2.1. Penalized boundary conditions

Characteristic-Base Volume Penalization imposes Dirichlet, Neumann, and Robin type boundary conditions by introducing forcing terms into the constitutive equations. Consider a domain Ω containing obstacles O_m, and governed by a generalized evolution equation

$$\frac{\partial u}{\partial t} = \text{RHS} \tag{1}$$

outside of O_m, where RHS is simply the physical right hand side forcing terms. Eq. (1) can be hyperbolic or parabolic in nature. A masking function, $\chi(\mathbf{x}, t)$, is defined across Ω, where

$$\chi(\mathbf{x}, t) = \begin{cases} 1 & \text{if } x \in O_m, \\ 0 & \text{otherwise}, \end{cases}$$

separates the domain into a physical region and a penalized region defined by the solid obstacle.

Dirichlet conditions are imposed in the same fashion as with the Brinkman penalization method [7,8]. For the boundary condition $u = u_0(\mathbf{x}, t)$ on an obstacle surface $\partial O_m(\mathbf{x}, t)$, the constitutive equation (1) is modified into the penalized equation

$$\frac{\partial u}{\partial t} = (1-\chi)\times \text{RHS} - \frac{\chi}{\eta_b}\big(u - u_0(\mathbf{x},t)\big) + \chi\,\nu_n \frac{\partial^2 u}{\partial x_i,\,\partial x_i}, \tag{2}$$

with summation implied over repeated indices. Convergence of the penalization parameter, as $\eta_b \to 0$, controls the error on the solution [2] by decreasing the timescale of the forcing term. Note that moving and deformable obstacles are defined in the penalized equation (2) by transient mask $\chi(\mathbf{x}, t)$ and boundary condition $u_0(\mathbf{x}, t)$ functions.

Typically, Brinkman penalization retains the constitutive equations inside of the obstacle and the penalization terms are simply appended where $\chi = 1$ [2]. The physical viscosity ensures smoothness and continuity of the solution. In departure from this convention, CBVP removes the physical terms, RHS, from within the obstacle in order to prevent secondary effects of coupled systems of equations from contaminating the desired boundary conditions. This allows for consistent control over the penalization scheme, regardless of the external physical terms.

In the formulation (2), removal of the constitutive equations from inside O_m necessitates the use of the penalized terms with nonphysical diffusion of strength ν_n in order to avoid creation of the discontinuous solution across the obstacle boundary. The use of numerical viscosity lends flexibility and generality to the method, as ν_n can be prescribed based on the particular numerical environment. Since continuous fluxes across the obstacle boundary are unnecessary, the diffusion term is not written in divergence form in order to enforce continuity through the first derivative. The use of a conservative viscous term across the discontinuous function $\chi\,\nu_n(x)$ would result in discontinuous derivatives at the interface of the obstacle.

Since the nonphysical diffusion contributes to boundary condition error, the coefficient ν_n is prescribed to be the minimal necessary for the stability of the numerical method. The diffusive length scale, which must be sufficiently resolved, can be determined through order of magnitude analysis considering diffusive strength ν_n and a penalization timescale of η_b. For a resolution of Δx within O_m, the diffusive coefficient must be $\nu_n \geqslant O(\Delta x^2/\eta_b)$.

The Neumann condition, $\partial u/\partial \mathbf{n} = q(\mathbf{x}, t)$ for inward-oriented surface normal $\mathbf{n} = n_k$, is imposed by introducing forcing upon the derivatives of u. Since the volume of the obstacle is penalized rather than just the surface, the surface normal is defined everywhere by linear extension throughout O_m. This leads to the penalized, hyperbolic equation

$$\frac{\partial u}{\partial t} = (1-\chi)\times \text{RHS} - \frac{\chi}{\eta_c}\left(n_k \frac{\partial u}{\partial x_k} - q(\mathbf{x},t)\right). \tag{3}$$

With the normal defined everywhere, (3) has inward-pointing characteristics that extend perpendicular to the surface into O_m. This propagates the solution from the surface inward with a spatial growth or decay, based on q, that enforces the desired derivative. The inward nature of the characteristics also prevents the nonphysical solution within O_m from propagating outwards, so that the external solution is only affected through the surface derivative imposed by penalization. Since the constitutive equations might also be hyperbolic, as in the case with compressible flows, removal of the physical right hand side terms from (3) ensures inward orientation of characteristics within the penalized region.

The Robin boundary condition, of the form $a(\mathbf{x}, t)u + b\partial u/\partial \mathbf{n} = g(\mathbf{x}, t)$ with $b > 0$, is similarly penalized through the hyperbolic equation

$$\frac{\partial u}{\partial t} = (1-\chi)\times \text{RHS} - \frac{\chi}{\eta_c}\left(a(\mathbf{x},t)u + b n_k \frac{\partial u}{\partial x_k} - g\right). \tag{4}$$

Here, the hyperbolic propagation is accompanied by an additional source term, au, indicating that the penalized Neumann condition (3) is simply a special case of the Robin condition where $a = 0$. For penalization, it is important that the Robin boundary condition is expressed so that b is positive, otherwise the characteristics within O_m will point outward. For simplicity, it is defined here as a constant.

It can easily be seen that at steady-state within O_m, both the Neumann- (3) and Robin-type (4) penalized equations converge on the surface to the desired boundary condition. Since the penalization timescale is controlled through the parameter η_c, selecting $\eta_c \ll 1$ causes (3) and (4) to become quasi-steady within O_m on the normalized problem timescale, therefore imposing the intended BC on the surface. As $\eta_c \to 0$, the increased disparity in timescales asymptotically controls the penalization error. However, reducing the error increases the computational complexity. Since $1/\eta_c$ is the characteristic velocity for (3), (4), a reduction of η_c is also accompanied by increased stiffness, a well known problem with Brinkman penalization that is mitigated through stiffly-stable solvers [7].

2.2. Stability and penalization of closed obstacles

In some cases, the hyperbolicity of penalized equations can lead to difficulties when (3) and (4) are applied across all of Ω. Since the characteristics all follow surface normals, a situation can arise for some geometry, including all closed obstacles, where characteristics converge and create inconsistencies and discontinuities. By defining the normal throughout the volume of O_m by the gradient of a scalar distance function,

$$\mathbf{n} = \nabla d, \tag{5}$$

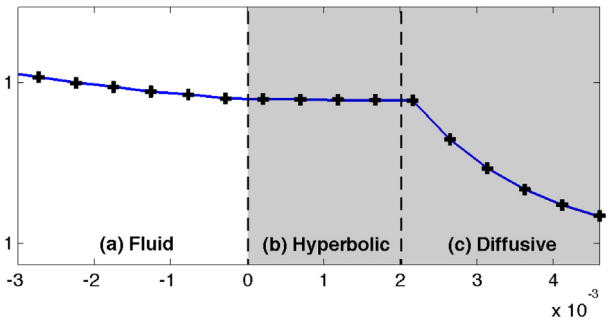

Fig. 1. A dual-zone penalization approach for resolving intersecting characteristics. An obstacle consists of hyperbolic (b) and diffusive (c) regions. The hyperbolic zone contains the CBVP terms and provides boundary condition support for the solid–fluid interface. The diffusive zone provides continuity throughout Ω.

where d is the distance to the nearest point on a surface, it can be seen that characteristics of (3) and (4) will converge wherever d is nondifferentiable. This occurs wherever a point inside O_m is equidistant from multiple surface points.

To circumvent this difficulty, local differential schemes can be implemented, if possible, and regions of intersecting characteristics omitted from the solution. For some solvers, like AWCM which employs global derivatives, this is not possible or practical. In such a case, inconsistencies with characteristics are avoided by only applying the hyperbolic terms in a narrow region along the surface within O_m, as shown in Fig. 1. This region is only wide enough to accommodate the differencing stencil for external points located immediately outside of the interface. Additional points within the obstacle are unnecessary to support external derivatives.

The interior region, where the hyperbolic penalization terms are not applied, is governed by weak diffusion to provide support for global derivatives. Unlike the diffusion used to stabilize the penalized Dirichlet condition (2), this diffusion is defined in conservative form, maintaining continuous fluxes throughout O_m.

Transition between the hyperbolic and the diffusive regions often introduces a discontinuous derivative. To avoid forming oscillations, the differencing stencil for hyperbolic terms must be prevented from crossing the transition and any potential discontinuities. Points near the transition employ upwind-biased differencing with fully upwind schemes immediately adjacent to the transition. Experience has shown that oscillations arising from ill-constructed zone transitions and exacerbated by penalization stiffness can propagate outward and degrade the physical solution in spite of the inward-pointing characteristics. The hyperbolicity does, however, prevent the solution in the diffusive region from affecting the solution on the obstacle surface. Using low-order, upwind-biased differencing and a narrow convective zone has the added benefit of increased stability with implicit methods, allowing calculations on the external, physical timescale.

These additional considerations of a dual zone approach emphasize the need to remove the physical terms within O_m from the penalized equations (2)–(4) to ensure that all characteristics point inward on the obstacle, regardless of the constitutive equations. Furthermore, retention of physical coupling within O_m could lead to steep gradients and other spurious structures contaminating other boundary conditions. Obstacles that employ both characteristic-based and Dirichlet-type penalization on separate variables are particularly susceptible to adverse coupling effects if physical terms are not removed.

3. Penalization of the Navier–Stokes equations

A principle strength of this method is the ability to easily prescribe boundary conditions in a systematic manner. Intentionally general, CBVP can be used for a variety of physical systems and evolution equations, including fluid regimes. Here penalization is applied for compressible, viscous flows around complex geometries.

3.1. Governing equations

The fluid is governed by the fully compressible Navier–Stokes equations. The nondimensionalized continuity, momentum and energy equations in conservative form are

$$\frac{\partial \rho}{\partial t} = -\frac{\partial \rho u_j}{\partial x_j}, \tag{6}$$

$$\frac{\partial \rho u_i}{\partial t} = -\frac{\partial (\rho u_i u_j)}{\partial x_j} - \frac{\partial p}{\partial x_i} + \frac{1}{Re_a}\frac{\partial \tau_{ij}}{\partial x_j}, \tag{7}$$

$$\frac{\partial \rho e}{\partial t} = -\frac{\partial}{\partial x_j}\left[(\rho e + p)u_j\right] + \frac{1}{Re_a}\frac{\partial (u_i \tau_{ij})}{\partial x_j} + \frac{1}{(\gamma - 1)}\frac{1}{Re_a Pr}\frac{\partial}{\partial x_j}\left(\mu \frac{\partial T}{\partial x_j}\right), \tag{8}$$

where

$$p = \frac{\rho T}{\gamma}, \tag{9}$$

$$\tau_{ij} = \mu\left(\frac{\partial u_i}{\partial x_j} + \frac{\partial u_j}{\partial x_i} - \frac{2}{3}\frac{\partial u_k}{\partial x_k}\delta_{ij}\right), \tag{10}$$

$$\mu = \frac{1+S_1}{T+S_1}(T)^{3/2}, \tag{11}$$

$$e = \frac{1}{2}u_i u_i + c_p T - \frac{p}{\rho}, \tag{12}$$

Re_a is the acoustic Reynolds number and Pr is the Prandtl number. Length scales are based on the characteristic length of the obstacle, L. The velocity $\mathbf{u}$ is nondimensionalized based on the reference speed of sound c_0, time based on L/c_0, specific energy on c_0^2, density on ρ_0, pressure on $\rho_0 c_0^2$, viscosity on μ_0, thermal conductivity on $\mu_0 c_{p_0}$, and temperature on T_0. Here, Sutherland's law is used for temperature-dependent viscosity, and the constant S_1 is normalized to the reference temperature.

For the benchmark problems considered in this paper, no-slip and adiabatic/heat flux conditions are imposed on velocity and temperature. These boundary conditions, and their corresponding penalization equations, are

$$u_i|_{\partial O_m} = u_{0i}, \qquad \frac{\partial u_i}{\partial t} = (1-\chi)\times \mathrm{RHS} - \frac{\chi}{\eta_b}(u_i - u_{0i}) + \chi\,\nu_n \frac{\partial^2 u_i}{\partial x_j \partial x_j}, \tag{13}$$

$$n_k \frac{\partial T}{\partial x_k}\bigg|_{\partial O_m} = q, \qquad \frac{\partial T}{\partial t} = (1-\chi)\times \mathrm{RHS} - \frac{\chi}{\eta_c}\left(n_k \frac{\partial T}{\partial x_k} - q\right), \tag{14}$$

where $u_{0i} = u_{0i}(\mathbf{x}, t)$ and $q = q(\mathbf{x}, t)$ for the generalized case of moving or deforming obstacles and inhomogeneous heat flux.

In order to apply these penalized boundary conditions to the constitutive equations (6)–(8), the equations of state (9)–(12) are used to determine consistent penalization of the integrated variables ρ, ρu, and ρe, from the native variables u and T. However, without appropriate penalized equation for ρ, the equations of state are under-constrained. Additionally, a penalized equation for density must be provided within O_m since ρ is solved across all of Ω. For exact boundary conditions, the Navier–Stokes equations are well posed through no-slip and heat-flux conditions, so the continuity equation is solved for density. The simplest approach, then, is to analogously retain the continuity equation inside of a penalized obstacle, however this was found by Liu and Vasilyev [7] to cause unacceptable errors. Therefore, the difficulty is to determine an additional penalized equation for ρ that accurately matches the problem physics at the interface without imposing additional constraints upon the flow.

There are two main approaches to evolutionary penalization, each with their own advantages. Physical models can be used within the penalized region to mimic the solution on the interface, or an evolutionary condition imposed that passively provides continuity and smoothness. Characteristic-based passive evolutionary conditions have the advantage of generality, though implementation involves time integration of an additional equation.

The passive evolutionary condition is built upon the CBVP Neumann condition (3). Due to the inward pointing characteristic, the solution on the interface is determined by fluid physics with the derivative imposed by the penalized volume of O_m. By using an inhomogeneous Neumann condition on ρ where the target derivative throughout O_m is the normal derivative on the surface, density becomes completely passive to the fluid physics. This is done by introducing an additional equation and taking advantage of the hyperbolicity of CBVP to extrapolate the density derivative from the solid–fluid interface into O_m along the surface normal by

$$\frac{\partial \Phi}{\partial t} = -\frac{\chi}{\eta_c} n_k \frac{\partial \Phi}{\partial x_k}, \tag{15}$$

where

$$\Phi = (1-\chi) n_k \frac{\partial \rho}{\partial x_k} + \chi \Phi. \tag{16}$$

Defining Φ across all of Ω provides the necessary boundary condition from ρ for the hyperbolic equation (15), which is solved only within O_m. In this way, density derivatives are physically determined outside of the obstacle via the continuity equation and extrapolated inside O_m by integrating (15). Therefore, Φ is fully passive to the physical solution.

Within the penalized region, Φ becomes the target for the inhomogeneous Neumann condition on ρ, yielding the evolutionary condition

$$\frac{\partial \rho}{\partial t} = (1-\chi)\times \mathrm{RHS} - \frac{\chi}{\eta_c}\left(n_k \frac{\partial \rho}{\partial x_k} - \Phi\right). \tag{17}$$

Since both the solution ρ and its first derivative are propagated along the inward characteristic, both are determined by the fluid physics. The flux, however, is discontinuous across the solid–fluid interface.

Consistent penalization of the integrated compressible variables ρu_i and ρe is easily determined from physical boundary conditions and the equations of state (9)–(12) by noting that

$$\frac{\partial \rho u_i}{\partial t} = u_i \frac{\partial \rho}{\partial t} + \rho \frac{\partial u_i}{\partial t}, \tag{18}$$

$$\frac{\partial \rho e}{\partial t} = e \frac{\partial \rho}{\partial t} + \rho u_i \frac{\partial u_i}{\partial t} + c_v \rho \frac{\partial T}{\partial t}. \tag{19}$$

The temporal derivatives of u_i, T, and ρ in (18) and (19) are defined by the penalized native variables (13), (14) and (17). Upon substitution and writing the equations in terms of integrated variables, the penalized equations become

$$\frac{\partial \rho}{\partial t} = (1-\chi) \times \text{RHS} - \frac{\chi}{\eta_c}\left[n_k \frac{\partial \rho}{\partial x_k} - \Phi \right], \tag{20}$$

$$\frac{\partial \rho u_i}{\partial t} = (1-\chi) \times \text{RHS} - \chi\left[\frac{1}{\eta_b}\rho(u_i - u_{0i}) - \rho \nu_n \frac{\partial^2 u_i}{\partial x_j \partial x_j} + \frac{1}{\eta_c} u_i \left(n_k \frac{\partial \rho}{\partial x_k} - \Phi \right) \right], \tag{21}$$

$$\begin{aligned} \frac{\partial \rho e}{\partial t} = (1-\chi) \times \text{RHS} - \chi\Bigg[& \frac{1}{\eta_c}\left(n_k \frac{\partial \rho e}{\partial x_k} \right) + \frac{\rho(u_j - u_{0j})u_j}{\eta_b} - \frac{\rho u_j}{\eta_c} n_k \frac{\partial u_j}{\partial x_k} - \rho u_j \nu_n \frac{\partial^2 u_j}{\partial x_i \partial x_i} \\ & - \frac{1}{\eta_c} e\Phi - \frac{1}{\eta_c} c_v \rho q \Bigg], \end{aligned} \tag{22}$$

where the physical RHS terms in (20)–(22) are the Navier–Stokes equations (6)–(8).

An alternative method of treating ρ within the penalized region is by actively matching the physics of the fluid. This eliminates the need for additional integrated equations. From the momentum equation (7), assuming that the error on the no-slip condition is sufficiently small, the derivative of the full normal stress at a solid surface is zero. Since volume penalization acts across all of O_m and not just on the surface, it is inappropriate to directly apply the Neumann condition on the normal stress as a third BC, as a spurious stress in the penalized region is required to ensure smoothness of the velocity solution across the interface. However, for flow regimes with a sufficiently small gradient in the normal shear stress, that is

$$O\left(\frac{1}{Re_a} \frac{\partial n_k \tau_{nn}}{\partial x_k} \right) \ll 1, \tag{23}$$

through order of magnitude analysis, the normal stress derivative can be approximated as

$$\left. \frac{\partial n_k \sigma_{nn}}{\partial x_k} \right|_{O_m} \approx n_k \left. \frac{\partial p}{\partial x_k} \right|_{O_m} \approx 0. \tag{24}$$

Attached boundary layer flows and linear acoustic regimes, among others, typically satisfy this criterion. A consistent boundary treatment for density can therefore be determined from (24), the equation of state (9), and the condition on temperature (14). As this condition attempts to match the fluid physics, violation of aforementioned assumptions leads to large errors and oscillations which are particularly problematic for adaptive grids.

For some of the problems presented in this paper, low viscosity and a stationary, adiabatic obstacle makes the problem well suited for imposing this normal stress approximation (24). Noting that the no-slip condition for a stationary obstacle can be expressed as $(\rho u)_{0i} = u_{0i} = 0$, the momentum equation can be directly penalized instead of velocity (13). By applying (24) as a third condition, the penalized Navier–Stokes equations are determined from (18) and (19) as

$$\frac{\partial \rho}{\partial t} = (1-\chi) \times \text{RHS} - \frac{\chi}{\eta_c}\left(n_k \frac{\partial \rho}{\partial x_k} \right), \tag{25}$$

$$\frac{\partial \rho u_i}{\partial t} = (1-\chi) \times \text{RHS} - \chi\left[\frac{1}{\eta_b}\rho u_i - \nu_n \frac{\partial^2 \rho u_i}{\partial x_j \partial x_j} \right], \tag{26}$$

$$\frac{\partial \rho e}{\partial t} = (1-\chi) \times \text{RHS} - \chi\left[\frac{1}{\eta_c}\left(n_k \frac{\partial \rho e}{\partial x_k} \right) + \frac{\rho u_j u_j}{\eta_b} - \frac{u_j}{\eta_c} n_k \frac{\partial \rho u_j}{\partial x_k} - u_i \nu_n \frac{\partial^2 \rho u_i}{\partial x_j \partial x_j} \right]. \tag{27}$$

This penalized system is more simple than (20)–(22), and does not require any additional integrated equations to calculate an evolutionary target ϕ. However, it is a form specific to a non-movable, non-deformable, adiabatic obstacle.

3.2. Error estimation from linear asymptotic analysis

While it is difficult to analyze convergence of the penalized Navier–Stokes equations directly, rigorous asymptotic analysis gives insight into the error of the penalization parameters η_b and η_c. Consider one-dimensional flow with an acoustic pulse reflecting off an obstacle. Error arising from the penalization can be examined in the fully reflected pulse.

For the entire domain, the amplitudes of the nondimensionalized flow variables are asymptotically expanded. The leading order expansions are identical in both cases where $\eta_b \ll \eta_c$ and $\eta_b \gg \eta_c$, so $\eta = \max(\eta_b, \eta_c) \ll 1$ to preserve generality. The leading perturbation terms for both the fluid and penalized regions are

$$\rho_f(x,t) = 1 + \epsilon\rho'_{0f} + \epsilon\eta\rho'_{1f} + \cdots, \qquad u_f(x,t) = \epsilon u'_{0f} + \epsilon\eta u'_{1f} + \cdots,$$
$$p_f(x,t) = \frac{1}{\gamma} + \epsilon p'_{0f} + \epsilon\eta p'_{1f} + \cdots, \qquad T_f(x,t) = 1 + \epsilon T'_{0f} + \epsilon\eta T'_{1f} + \cdots. \tag{28}$$

For the fluid region, where $\chi = 0$, substitution into (25)–(27) and retaining only first order terms, in essence linearizing the equations, yields the system

$$\frac{\partial u'_f}{\partial t} + \frac{\partial p'_f}{\partial x} = 0, \tag{29}$$
$$\frac{\partial p'_f}{\partial t} + \frac{\partial u'_f}{\partial x} = 0, \tag{30}$$

for both zero- and first-order perturbation quantities. Viscous terms are neglected in the high Reynolds number limit, where $1/Re_a \ll \eta$. Additionally, the relation $\rho'_f = p'_f$ holds, and the flow is isentropic. The resulting system (29), (30) is simply the linear acoustic equations, describing small amplitude pulses propagating through the fluid.

For the penalized region, where $\chi = 1$, substitution of the asymptotically expanded variables into (25)–(27) and retaining first order perturbation quantities yields

$$\frac{\partial \rho'_p}{\partial t} + \frac{1}{\eta_c}\frac{\partial \rho'_p}{\partial n} = 0, \tag{31}$$
$$\frac{\partial u'_p}{\partial t} + \frac{1}{\eta_b}u'_p - \nu_n\frac{\partial^2 u}{\partial x^2} = 0, \tag{32}$$
$$\frac{\partial p'_p}{\partial t} + \frac{1}{\eta_c}\frac{\partial p'_p}{\partial n} = 0. \tag{33}$$

Again, the isentropic relation $\rho'_f = p'_f$ holds.

The perturbation equations (31)–(33) form a linear hyperbolic system of PDEs with a single characteristic pointing inward on the penalized domain. Strong damping on velocity drives the solution towards the no-slip condition on timescale η_b, while strong convection on timescale η_c enforces the desired Neumann conditions. This implies $\eta_b < \eta_c$ to avoid excessive phase lag in reflected pulses as energy and mass are convected too quickly past the interface.

In order to examine the error convergence as $\eta_b, \eta_c \to 0$, the two systems (29), (30) and (31)–(33) are solved on a one-dimensional split domain. Fluid occupies the semi-infinite region $x < 0$ while $x \geqslant 0$ is penalized, placing the solid interface at the origin.

The D'Alembert solution in the fluid region, in terms of initial $(u'_0(x), p'_0(x))$ conditions and boundary values $(u'_1(t), p'_1(t))$ at the fluid–obstacle interface, is

$$u'_f(x,t) = \frac{1}{2}u'_0(x-t) + \frac{1}{2}p'_0(x-t) + \frac{1}{2}u'_1(x+t) - \frac{1}{2}p'_1(x+t), \tag{34}$$
$$p'_f(x,t) = \frac{1}{2}u'_0(x-t) + \frac{1}{2}p'_0(x-t) - \frac{1}{2}u'_1(x+t) + \frac{1}{2}p'_1(x+t), \tag{35}$$

for both zero- and first-order perturbations.

The solution in the penalized region can be determined for each variable independently. The first order perturbation of pressure is easily solved based on the propagation of the solution on the interface p'_1 for a single characteristic with speed $\lambda = \frac{1}{\eta_c}$,

$$p'_p(x,t) = p'_1(t - \eta_c x). \tag{36}$$

The first order velocity perturbation of u'_p can be solved by transforming (32) into the form of an inhomogeneous heat equation through

$$w'(x,t) = e^{-\frac{t}{\eta_b}}\left(u'(x,t) - u'(0,t)\right). \tag{37}$$

Assuming continuity with the fluid domain through the first derivative, the solution of $w'(x,t)$ on the semi-infinite domain is known [16]. Provided that the limits of the solution are finite and constant as $x \to 0$ for parameter η_b, then the solution at the interface is $O(\eta_b)$, and normalized to $u^*(t) = (\nu_n\eta_b)^{-1}u'_p|_{x=0}$. Now considering the acoustic timescale $1 \gg \eta_b$, the quasi-steady state solution to the boundary value problem (32) is found to be

$$u'_p(x,t) = \eta_b u^*(t)\exp\left(\frac{x}{\sqrt{\eta_b\nu_n}}\right). \tag{38}$$

Enforcing continuity and smoothness between the fluid domain (30), (29) and penalized domain solutions (36), (38) yields the acoustic solution with leading error terms

$$E = -\frac{1}{1-2\eta_c}\left[\eta_c\big(u_0'(-x-t)+p_0'(-x-t)\big)+\frac{\sqrt{\nu_n\eta_b}}{2}\int_0^{x+t}u^*(\xi)\,d\xi+\cdots\right], \tag{39}$$

on the reflected pulse for both p_f' and u_f'. The error due to the penalized Neumann condition on p is in phase with the reflected pulse, while both phase and amplitude error are introduced through the no-slip condition. The total error on $O(\eta_c, \eta_b^{1/2})$ reinforces that, optimally, the penalization parameters should be chosen so that $\eta_b < \eta_c$.

4. Numerical results

An initial examination into the accuracy of each CBVP boundary condition is obtained through numerical simulation of the one-dimensional diffusion equation. Each boundary condition type can be applied individually and in a physically meaningful way. The fluid benchmark problems here encompass a representative set of various flow regimes. One-dimensional acoustic reflection provides error convergence that corresponds to the analytic asymptotic analysis. Penalization is also applied for a multidimensional closed obstacle with flow past a cylinder. A low-compressibility, steady state benchmark is given, as well as compressible vortex shedding to demonstrate unsteady flow regimes. Both homogeneous and inhomogeneous Neumann conditions are implemented.

4.1. Benchmark I: One-dimensional diffusion

Consider transient one-dimensional diffusion across a domain, $\Omega = [-0.25, 0.015625]$, with the penalized obstacle at $O = [0, 0.015625]$. The parabolic equation

$$\frac{\partial u}{\partial t} = k\frac{\partial^2 u}{\partial x^2}, \tag{40}$$

is penalized by

$$\frac{\partial u}{\partial t} = (1-\chi)k\frac{\partial^2 u}{\partial x^2} - \frac{\chi}{\eta_b}(u-U_0) + \chi\nu_n\frac{\partial^2 u}{\partial x^2}, \tag{41}$$

$$\frac{\partial u}{\partial t} = (1-\chi)k\frac{\partial^2 u}{\partial x^2} - \frac{\chi}{\eta_c}\left(\frac{\partial u}{\partial n}-q\right), \tag{42}$$

$$\frac{\partial u}{\partial t} = (1-\chi)k\frac{\partial^2 u}{\partial x^2} - \frac{\chi}{\eta_c}\left(au+b\frac{\partial u}{\partial n}-g\right) \tag{43}$$

for Dirichlet, Neumann, and Robin conditions, respectively. The penalized diffusion equation for the Dirichlet condition (41) has been solved analytically by Kevlahan and Ghidaglia [4], though in the context of Stokes flow, so here we only consider the characteristic-based penalization BCs, (42) and (43). At the solid boundary, the conditions $\partial u/\partial x = 0$ and $u + 2\partial u/\partial x = 5$ are applied for the Neumann and Robin cases, respectively. At $t = 0$, an impulsive step function of height $\delta u = 1$ is applied at $x = 0$ and allowed to diffuse across the domain. The error is determined while the solution at the interface, $u(x = 0)$, is still transient.

This problem uses a nonadaptive grid of $M = 1089$ points. In determining the error, the solution is compared with numerical results with the exact boundary condition imposed and while the solution is still transient. The diffusive coefficient k were 0.5 and 1.0 for the Neumann- and Robin-type penalization respectively.

For comparison, the penalization for the Dirichlet condition converges as $O(\eta_b^{1/2})$ [4]. The error from penalization for both the Neumann and Robin conditions, in Fig. 2 converges as $O(\eta_c)$. This is expected, as the Neumann condition is simply a special case of the Robin, where $a = 0$, and the convective behavior of both penalized equations is a fundamental departure from Brinkman penalization of the Dirichlet condition. The parameter η_c is not representative of a modeled porosity or impedance, but simply a disparate timescale for the relaxation of the internal zone. The lower convergence rate for the Dirichlet condition is a consequence of the penalization terms forming a boundary layer inside of the obstacle in the immediate vicinity of the boundary.

4.2. Benchmark II: One-dimensional acoustic reflection

To examine the error convergence for the Navier–Stokes equations, where two penalization types are imposed on coupled equations, consider one-dimensional acoustic reflection. Isentropic, low amplitude pulses bounce off of a solid obstacle, and the mass and energy losses from penalization observed in the reflected pulse. The penalized equations are solved on

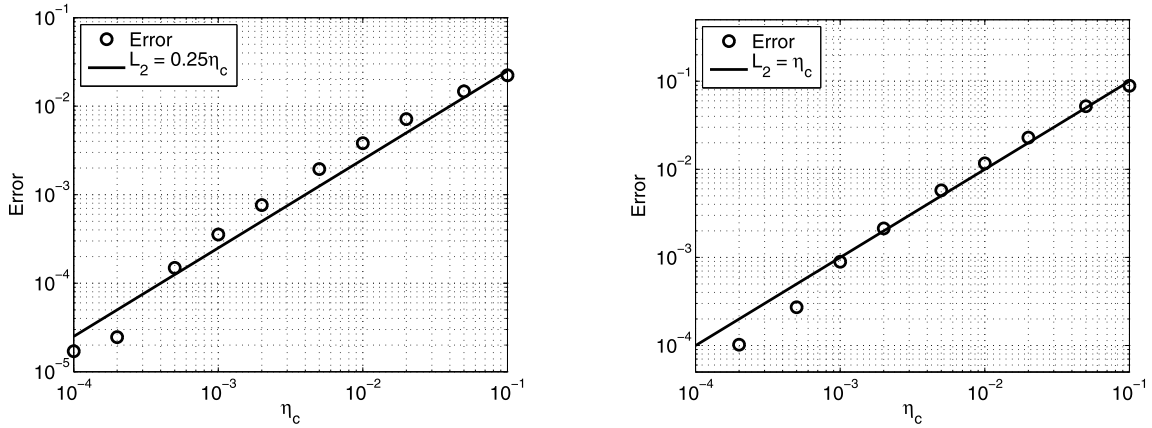

(a) Neumann (b) Robin

Fig. 2. Time-averaged L_2-norm error for converging η_c for Neumann (a) and Robin (b) conditions for 1D diffusion.

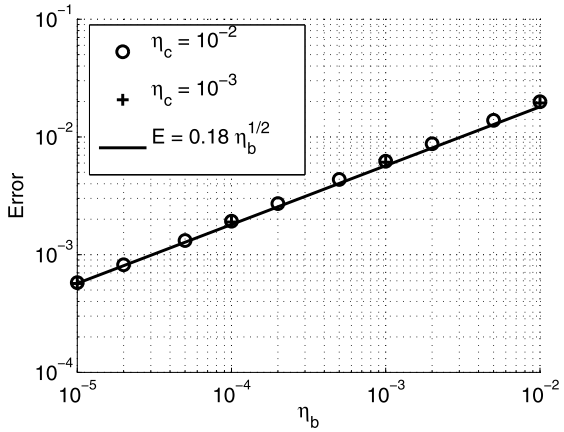

Fig. 3. L_2-norm error of a fully reflected pulse where η_c is held constant.

a domain $\Omega = [-0.65, 0.25]$, where the fluid occupies $\Omega_f = [-0.65, 0)$, and the solid obstacle is $O = [0, 0.25]$. The initial conditions consist of a localized pulse

$$\rho' = \rho u' = p' = 10^{-3}\left(\frac{x+0.25}{0.2} - 1\right)^4\left(\frac{x+0.25}{0.2} + 1\right)^4, \tag{44}$$

$$-0.45 < x < -0.05. \tag{45}$$

The high order polynomial ensures that the piecewise function is continuous through the second derivative, avoiding discontinuous fluxes. This problem is solved in the inviscid limit, $Re_a = 10^8$, and at a very fine resolution with $M = [235930]$ points at the highest adaptive level. To observe proper error convergence, the Brinkman diffusion term, ν_n, is held constant at $\nu_n = 20\Delta x$, which allows for convergence of η_b across several orders of magnitude on this grid.

No-slip and adiabatic conditions are penalized at the solid interface. Since the viscosity is negligible for this problem, the approximation $\partial P/\partial x = 0$ provides the evolution condition for density at the interface, and the simplified form of penalized equations, (25)–(27), are used.

Fig. 3 shows the error convergence on a fully reflected pulse for $\eta_b = [10^{-5}, 10^{-2}]$ where η_c is held constant at $\eta_c = 10^{-2}$ and 10^{-3}. The error convergence of both cases is the same, namely $O(\eta_b^{1/2})$, and neither case manifests significant errors from the characteristic-based terms. With the low amplitude, isentropic pulses and the inviscid limit, the asymptotic acoustic problem solved previously is well modeled here. The solution (39) indicates an in-phase error that is highly localized with a magnitude based on the initial pulse. At the pulse peak, the predicted error is $O(\eta_c)$ and rapidly diminishes with the local waveform amplitude. Therefore, the L_2-norm error of the numerical solution is dominated by the phase lag consequential of the no-slip condition, even at $\eta_b = 10^{-5}$. This result demonstrates that reasonable error convergence can be achieved through only moderate values of η_c. This is beneficial as it mitigates the computational costs associated with the stiffness of the hyperbolic penalization terms.

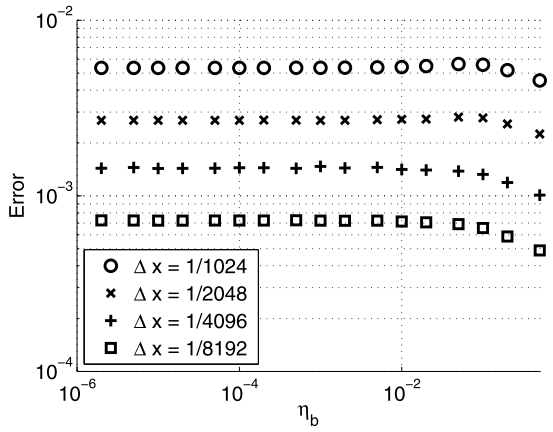

Fig. 4. L_2-norm error of a fully reflected pulse where numerical viscosity within the obstacle is $\nu_n = \alpha^2 \Delta x^2 / \eta_b$. With $\nu_n = f(1/\eta_b)$, the error demonstrates an insensitivity to the penalization parameter, but is rather controlled by the resolution as $O(\Delta x)$.

An alternative to a constant ν_n is to set the coefficient based on the penalization timescale and resolution to ensure that diffusive effects are properly resolved. For α grid points in the diffusive length scale,

$$\nu_n = \frac{\alpha^2 \Delta x^2}{\eta_b}. \tag{46}$$

Experience has shown that $\alpha = O(1)$ points is the minimum required to avoid adaptive mesh-saturating oscillations using AWCM. With η_c and Δx remaining constant, the error on a fully reflected pulse does not converge with η_b, as shown in Fig. 4. A reduction in η_b is met with a proportional increase in ν_n, resulting in an error that is insensitive to the penalization parameter. Rather, the error converges as $O(\Delta x)$. This agrees well with the result of the asymptotic analysis (39), which predicts an error of $O(\eta_b^{1/2} \nu_n^{1/2})$. By defining ν_n as in (46), the predicted error is $O(\alpha \Delta x)$. Since α is based on how well a solver tolerates under-resolved features, this approach effectively minimizes the error while robustly preserving stability. The assumption still holds that η_b is much smaller than the normalized timescale of the fluid, however further reduction becomes superfluous and the error is set by the resolution of the grid near the interface.

4.3. Benchmark III: Low Mach number external flow

To extend CBVP to multiple dimensions, incompressible flow past a circular cylinder is considered. For steady flow, with $Re \leqslant 40$, the boundary layer behavior in the wake of a circular cylinder is well documented for both experimental and numerical cases [17–22]. Since the streamlines are curved at the interface, the freestream Reynolds number is low, and the boundary layer separates from the trailing edge, the approximation $\partial P / \partial \mathbf{n} \approx 0$ breaks down and the simplified penalization (25)–(27) is no longer valid. Instead, the more robust form of the penalized Navier–Stokes equations, (20)–(22), using a characteristic-based evolutionary condition on ρ. For accurate simulation of boundary layer separation, the proper treatment of the pressure gradient at the surface is important.

The flow is modeled as weakly compressible with $Ma = 0.03$ and freestream Reynolds number of $Re = 40$. A cylinder with radius $r = 0.5$ ($D = 1.0$) is centered on the origin of domain $\Omega = [-5, 10] \times [-5, 5]$, and the penalization parameters are $\eta_b = 5 \times 10^{-3}$ and $\eta_c = 10^{-2}$. The numerical viscosity is set according to (46), so that penalization error is automatically minimized based upon the highest resolution of the adaptive grid. Several different resolutions are used to demonstrate the control of the error through ν_n. Four cases are considered, where the maximum level of resolution on the adaptive grid is $\Delta x = 1/256, 1/512, 1/1024$, and $1/2048$. The boundary layer separation point, θ, and the separated wake length L are both measured from the trailing edge of the cylinder.

Flow field velocity at steady state is shown in Fig. 5. The results for each level of resolution are summarized in Table 1 and compared with previous numerical and experimental results. For increasingly refined grids, the solution converges to previously established values [17–22]. The error arising from the no-slip condition manifests as a nonzero velocity on the surface, delaying boundary layer separation and decreasing the drag on the surface. By increasing the resolution, the viscous lengthscale decreases and with it the slip error at the surface. The large nu_n dependency and the high accuracy for moderate η_c reinforces that the error on the penalized Dirichlet condition remains the limiting factor.

4.4. Benchmark IV: Laminar vortex shedding

To verify the efficacy of CBVP for unsteady solutions, CBVP is applied for low Reynolds number vortex shedding around a two-dimensional cylinder. For $Ma = 0.20$ and $Re = 1000$, the flow past a cylinder remains laminar but experiences vortex shedding from the trailing edge. The domain discretization and penalization parameters remain as for the

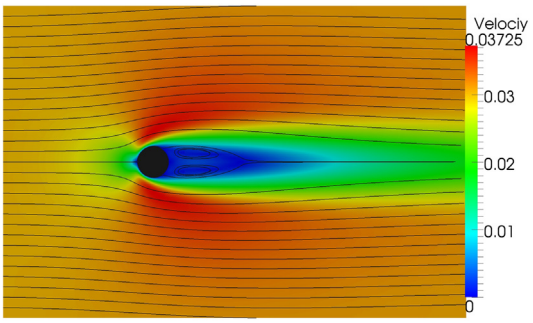

Fig. 5. Velocity magnitude and streamlines at steady state for $Re = 40$ and $Ma = 0.03$.

Table 1
Numerical results for incompressible/pseudo-incompressible flow past a 2D cylinder at $Re = 40$. The separation point Θ and drag coefficient C_D from a CBVP obstacle can be seen converging to previously established results as grid spacing, and therefore nonphysical viscosity, are reduced. The far field flow, as indicated by the separated wake length, is largely unaffected. Note that the wake length L determined by Coutanceau and Bouard [17] is extrapolated at $Re = 40$.

	Θ	L	C_D
Experimental			
Coutanceau and Bouard [17]	53.8°	2.11*	–
Tritton [18]	–	–	1.54
2D Numerical			
Linnick and Fasel [19]	–	2.28	1.54
Dennis and Chang [20]	53.8°	2.35	1.52
Fornberg [21]	55.6°	2.24	1.50
de Tullio et al. [22]	53.7°	2.23	1.49
Present			
$\Delta x = \frac{1}{256}$	**51.6°**	**2.31**	**1.47**
$\Delta x = \frac{1}{512}$	**52.8°**	**2.31**	**1.48**
$\Delta x = \frac{1}{1024}$	**53.7°**	**2.30**	**1.48**
$\Delta x = \frac{1}{2048}$	**53.6°**	**2.28**	**1.51**

pseudo-incompressible case, namely $\Omega = [-5, 10] \times [-5, 5]$, $\eta_b = 5 \times 10^{-3}$ and $\eta_c = 10^{-2}$. Density is penalized with the evolutionary condition (17), and two temperature conditions are considered: an adiabatic cylinder and constant heat flux at $\partial T/\partial \mathbf{n} = 1.5$.

The velocity and vorticity fields around an adiabatic cylinder are shown in Fig. 6, as well as the temperature for both the adiabatic and heated cylinders. Periodic vortex shedding can be seen in the laminar wake behind the cylinder.

In the case of the heated cylinder, the constant flux causes a temperature rise $O(0.1)$ along the surface. While Wang et al. [23] predict a decrease in the shedding frequency for a heated cylinder at low Reynolds number, the Strouhal number here is essentially unchanged by the increased temperatures. For laminar flows in the region of $Re \approx 1000$, the frequency is insensitive to the Reynolds number [24]. The increase in temperature, and corresponding increase in viscosity, is therefore insufficient to decrease the local Reynolds number enough to affect the periodicity of the wake. The heating is then best seen only through the direct effect on the temperature of the fluid. Examination of the temperature profile along an arbitrary surface normal, shown in Fig. 7, verifies that the desired heat-flux of $q = 1.5$ is properly enforced on the penalized boundary.

Time variant lift and drag coefficients C_L and C_D, shown in Fig. 8, and agree well with previous numerical results [24], though a slightly shorter shedding period can be seen. This higher frequency is reflected in a Strouhal number of $St = 0.245$, compared to $St = 0.238$ determined by Brentner et al. [24].

4.5. Benchmark V: Moving cylinder

One of the advantages of volume penalization is the ability to easily model moving and deformable obstacles. In order to demonstrate CBVP for moving obstacles, external flow around a cylinder is considered in stationary and moving inertial reference frames. For both cases, the flow parameters remain the same, namely $Ma = 0.1$ and $Re = 185$, where the reference velocity is the difference between the cylinder and freestream. They use an effective resolution of $\Delta x = \Delta y = 1/512$, and penalization parameters $\eta_b = 10^{-2}$ and $\eta_c = 10^{-1}$. The stationary inertial frame is solved on a domain $\Omega = [-7, 12] \times [-7, 7]$, proceeding until steady periodic vortex shedding is established.

In the moving reference frame, the freestream velocity is halved with respect to the computational grid and the obstacle translated upstream and an equal rate. The result is an inertial frame moving at $u_{\text{inf}}/2$ in the positive x-direction compared

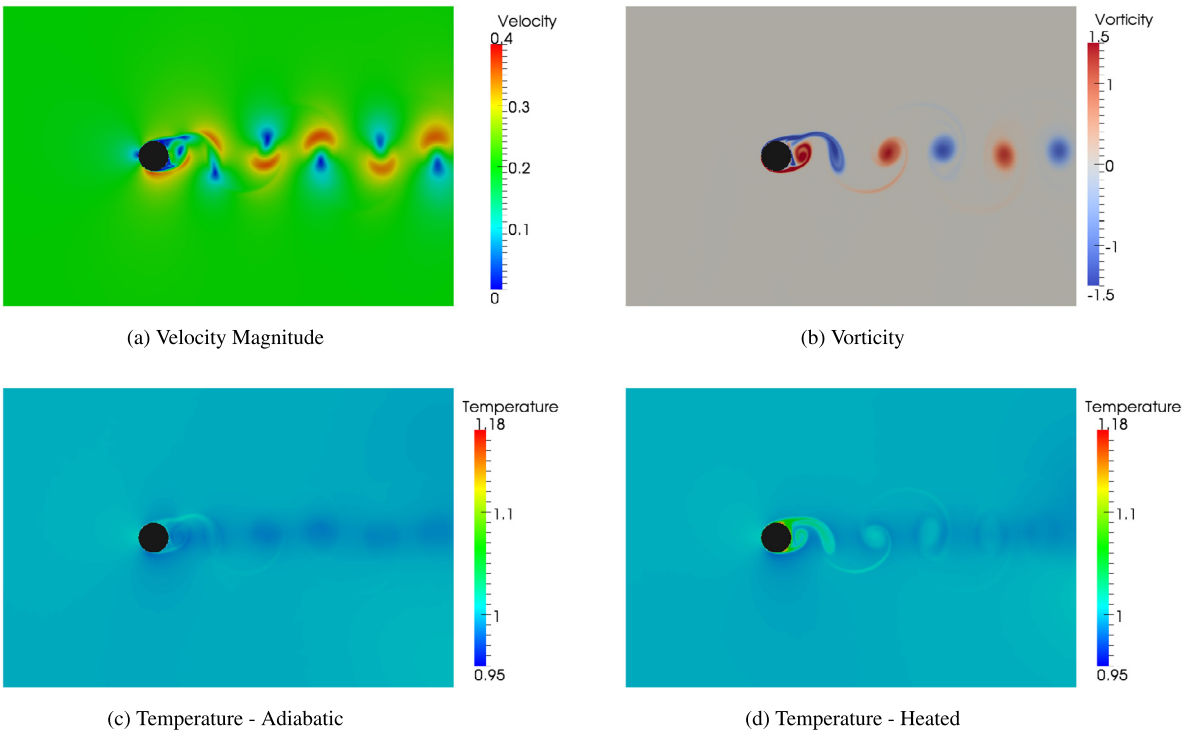

(a) Velocity Magnitude

(b) Vorticity

(c) Temperature - Adiabatic

(d) Temperature - Heated

Fig. 6. Velocity (a) and vorticity (b) field for flow around an adiabatic cylinder at $Re = 1000$. The Kàrmàn vortex street is clearly visible. The temperature fields are also shown for an adiabatic (c) and heated (d) cylinder, where the nondimensional heat-flux is $q = 1.5$.

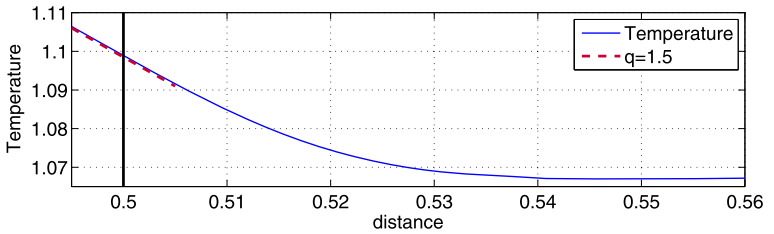

Fig. 7. Temperature profile along the surface normal at $\theta = \pi/4$, measured from the trailing edge. The imposed Neumann condition $\partial T/\partial \mathbf{n} = q = 1.5$ has been penalized at the surface. The distance along the profile is measured from the center of the cylinder, where the surface is at 0.5.

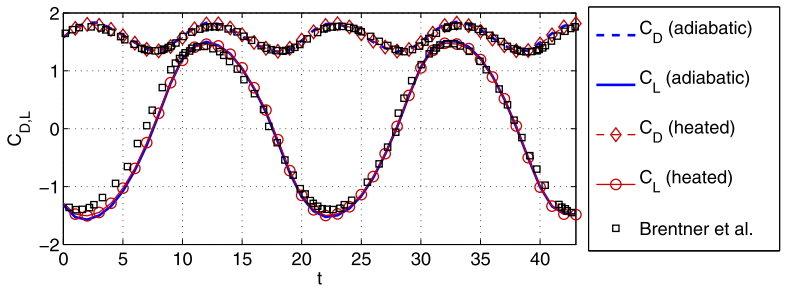

Fig. 8. Lift and drag coefficients, C_L and C_D, for unsteady flow at $Re = 1000$ compared to those of Brentner et al. [24]. The results presented here agree well, however a slight discrepancy can be seen in a slightly higher shedding frequency.

to the stationary case. This case is solved on a domain $\Omega = [-22, 7] \times [-7, 7]$ with the same effective resolution. Due to limitations on the total simulation time that are imposed by the domain length, a statistically steady state was unable to be verified. However, comparison of the transient force coefficients C_L and C_D in Fig. 9 show excellent agreement between late periodic shedding in the moving frame and the statistically steady shedding in the stationary frame.

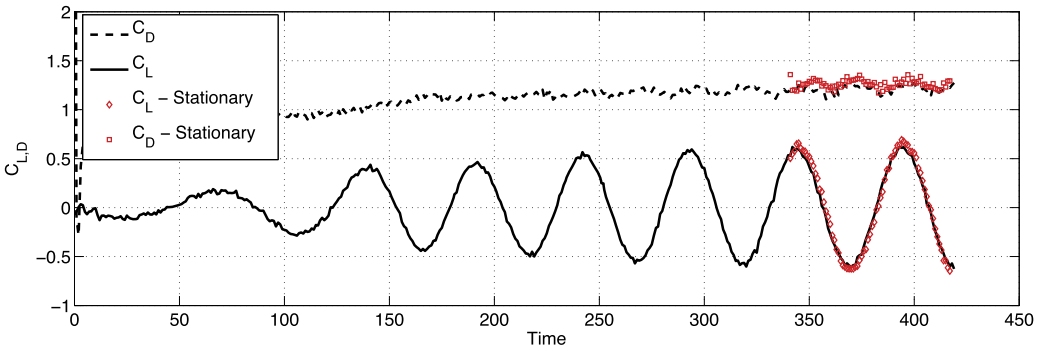

Fig. 9. Lift and drag coefficients, C_L and C_D, for flow around an impulsively started moving cylinder at $R = 185$. The statistically steady force coefficients for the case solved in an inertial frame of a stationary obstacle are shown for comparison, once periodic shedding is established.

5. Conclusions

A new volume penalization method has been introduced here to extend Brinkman penalization to generalized Neumann and Robin conditions for hyperbolic and parabolic equations. This is accomplished through hyperbolic penalization terms whose characteristics point inward along the surface-normal direction. The process of prescribing BCs is flexible, and constructing problem-specific schemes is systematic through penalization of native variables and propagating to the integrated equations. Multiple approaches to evolutionary boundary conditions, such as the treatment of the density for compressible flows, were developed using CBVP. Such quantities can be either actively modeled and the physics matched at the solid–fluid interface, or evolved passively making full use of the hyperbolicity of CBVP to propagate physical derivatives.

As with Brinkman penalization, the error of CBVP was shown to be rigorously controlled through the penalization parameter, η. The error from penalized Neumann and Robin Conditions converges as $O(\eta_c)$. With a more favorable convergence than the Brinkman-based penalized Dirichlet condition, which converges as $O(\eta_b^{1/2})$, application to the compressible Navier–Stokes equations typically found the accuracy to be dependent upon the error of the no-slip condition and insensitive to Neumann parameters. In this way, a comprehensive method of imposing general boundary conditions is introduced without significantly impacting the error vis-à-vis the well-vetted Brinkman penalization. The higher order error of CBVP is especially important considering the additional stiffness that accompanies the hyperbolic terms.

Acknowledgements

This work was supported by ONR MURI on Soil Blast Modeling under Grant No. N00014-11-1-069 and utilized the Janus supercomputer, which is supported by the National Science Foundation (award number CNS-0821794) and the University of Colorado Boulder. The Janus supercomputer is a joint effort of the University of Colorado Boulder, the University of Colorado Denver and the National Center for Atmospheric Research.

References

[1] R. Mittal, G. Iaccarino, Immersed boundary methods, Annu. Rev. Fluid Mech. 37 (2005) 239–261.
[2] P. Angot, C.-H. Bruneau, P. Fabrie, A penalization method to take into account obstacles in viscous flows, Numer. Math. 81 (1999) 497–520.
[3] E. Feireisl, J. Neustupa, S. Stebel, Convergence of a Brinkman-type penalization for compressible fluid flows, J. Differ. Equ. 250 (2011) 596–606.
[4] N.-R. Kevlahan, J.-M. Ghidaglia, Computation of turbulent flow past an array of cylinders using a spectral method with Brinkman penalization, Eur. J. Mech. B, Fluids 20 (2001) 333–350.
[5] R. Pasquetti, R. Bwemba, L. Cousin, A pseudo-penalization method for high Reynolds number unsteady flows, Appl. Numer. Math. 58 (2007) 946–954.
[6] C. Jause-Labert, F. Godeferd, B. Favier, Numerical validation of the volume penalization method in three-dimensional pseudo-spectral simulations, Comput. Fluids 67 (2012) 41–56.
[7] Q. Liu, O. Vasilyev, Brinkman penalization method for compressible flows in complex geometries, J. Comput. Phys. 227 (2007) 946–966.
[8] O. Vasilyev, N.-R. Kevlahan, Hybrid wavelet collocation-Brinkman penalization method for complex geometry flows, Int. J. Numer. Methods Fluids 40 (2002) 531–538.
[9] I. Ramière, P. Angot, M. Belliard, A fictitious domain approach with spread interface for elliptic problems with general boundary conditions, Comput. Methods Appl. Mech. Eng. 196 (2007) 766–781.
[10] O. Boiron, G. Chiavassa, R. Donat, A high-resolution penalization method for large Mach number flows in the presence of obstacles, Comput. Fluids 38 (2009) 703–714.
[11] Y. Bae, Y. Moon, On the use of Brinkman penalization method for computation of acoustic scattering from complex boundaries, Comput. Fluids 55 (2012) 48–56.
[12] B. Kadoch, D. Kolomenskiy, P. Angot, K. Schneider, A volume penalization method for incompressible flows and scalar advection–diffusion with moving obstacles, J. Comput. Phys. 231 (2012) 4365–4383.
[13] O. Vasilyev, Solving multi-dimensional evolution problems with localized structures using second generation wavelets, in: Special Issue on High-Resolution Methods in Computational Fluid Dynamics, Int. J. Comput. Fluid Dyn. 17 (2003) 151–168.
[14] O. Vasilyev, S. Paolucci, A dynamically adaptive multilevel wavelet collocation method for solving partial differential equations in a finite domain, J. Comput. Phys. 125 (1996) 498–512.

[15] O.V. Vasilyev, D.A. Yuen, S. Paolucci, The solution of PDEs using wavelets, Comput. Phys. 11 (1997) 429–435.
[16] J.R. Cannon, The One-Dimensional Heat Equation, Addison–Wesley, 1984.
[17] M. Coutanceau, R. Bouard, Experimental determination of the main features of viscous flow in the wake of a circular cylinder in uniform translation. Part 1. Steady flow, J. Fluid Mech. 79 (1977) 231–256.
[18] D. Tritton, Experiments on the flow past a circular cylinder at low Reynolds numbers, J. Fluid Mech. 6 (1959) 547–567.
[19] M.N. Linnick, H.F. Fasel, A high-order immersed interface method for simulating unsteady incompressible flows on irregular domains, J. Comput. Phys. 204 (2005) 157–192.
[20] S. Dennis, G.-Z. Chang, Numerical solutions for steady flow past a circular cylinder at Reynolds numbers up to 100, J. Fluid Mech. 42 (1970) 471–489.
[21] B. Fornberg, A numerical study of steady viscous flow past a circular cylinder, J. Fluid Mech. 98 (1980) 819–855.
[22] M. de Tullio, P.D. Palma, G. Iaccarino, G. Pascazio, M. Napolitano, An immersed boundary method for compressible flows using local grid refinement, J. Comput. Phys. 225 (2007) 2098–2117.
[23] A.-B. Wang, Z. Trávníček, K.-C. Chia, On the relationship of effective Reynolds number and Strouhal number for the laminar vortex shedding of a heated circular cylinder, Phys. Fluids 12 (2000) 1401–1410.
[24] K. Brentner, J. Cox, C. Rumsey, B. Younis, Computation of sound generated by flow over a circular cylinder: an acoustic analogy approach, in: C. Tam, J. Hardin (Eds.), Second Computational Aeroacoustics (CAA) Workshop on Benchmark Problems, in: NASA Conf. Publ., vol. 3352, NASA, 1997, pp. 289–295.